The Improved Dual Active Bridge Converter with a Modified Phase Shift and Variable Frequency Control

Feilong Liu, Xiaofeng Sun, Jia Feng, Junjuan Wu and Xin Li
Key Lab of Power Electronics for Energy Conservation and Motor Drive of Hebei Province
College of Electrical Engineering, Yanshan University
Qinhuangdao 066004, China
Email: {sxf,wujunjuan,yddylixin}@ysu.edu.cn, 910719169@qq.com, fengjia33536689@163.com

***Abstract*—This paper proposes a modified control scheme based on the dual active bridge converter with a center-tapped transformer. The tripe phase shift and fixed frequency (TPSFF) control is adopted to make sure that the soft-switching current of the switch bridge which is hardest to achieve soft switching is the fixed value at the light load. With the extended phase shift and variable frequency (EPSVF) control at the heavy load, not only the soft-switching current of the hardest switch bridge is the fixed value, but also the reactive power is restricted. And then, a 1.1kW experimental prototype is established to verify the correctness of theoretical analyses.**

Keywords—Dual active bridge; bidirectional DC-DC converter; center-tapped transformer; soft-switching; variable frequency

I. INTRODUCTION

Dual active bridge (DAB) converter can transmit power between two DC power supplies with different voltage levels. Therefore, the dual active bridge is widely used in the field which contains low voltage battery and high voltage bus, such as micro grid, electrical vehicles and uninterrupted power system. Compared with the traditional unidirectional DC\DC converter, the dual active bridge converter has the characteristics of less switching devices, bidirectional power transmission, easy to achieve soft switching, insensitive to parasitic parameters and so on. Thus far, dual active bridge converter is developing towards the following aspects: wide input or output voltage range, high voltage gain, wide soft-switching range, higher power density, and higher efficiency[1-2].

The classical control schemes of DAB involve the following aspects: 1) traditional single phase shift (SPS) control, 2) extended phase shift (EPS) control, 3) triple phase shift (TPS) control. SPS control is easy to realize the bidirectional power transmission only by adjusting the phase shift angle between the primary and secondary switch bridges and can make sure the converter obtain large power. However, SPS control restricts the input and output voltage range and the converter is difficult to achieve soft switching when the voltage gain deviates from the transformer ratio or at light load. What is more, the reactive power is protruded at the heavy load[3-8]. The EPS control broadens the input or output voltage range and improves the reactive power problem. And all switches can realize theoretical soft switching over full-operating range. Taking the parasitic capacitor of the switch into consideration, EPS control cannot provide enough soft-switching current at light load and the reactive power becomes too large with the increase of the phase shift between the primary and secondary switch bridges at heavy load[9-13]. TPS control can control the inductor current more precisely, and thus the root-mean-square (RMS) of the inductor current is optimized. However, the soft-switching current at light load is also not large enough and the converter cannot realize the soft switching[14-16]. With EPS or TPS control, the maximum power level of the system becomes lower with the same converter parameters and the control complexity increases. Based on the above study situation, some researchers have proposed hybrid phase shift (HPS) scheme.

Reference [17] proposed an improved dual active bridge converter with a center-tapped transformer. Considering the parasitic capacitor, all switches of the converter can achieve actual soft switching and the worst soft-switching current is the fixed value at light load with the TPS control when the voltage gain of the converter is double. However, TPS control cannot restrict the reactive current at heavy load.

This paper proposes a modified control scheme based on the improved dual active bridge converter. In terms of the volt-second balance of the transformer windings within half switching cycle, the TPSFF control can provide sufficient soft-switching current flowing through the center-tapped inductor by adjusting the secondary phase shift angle at light load. The EPSVF control can control the soft-switching current result that the current can be limited by adjusting the switch frequency at heavy load. Thus, the worst soft-switching current can be set as fixed value with full-operating range and the reactive power is controlled at heavy load.

II. OPERATION PRINCIPLE

Fig. 1 shows the topology of the improved DAB converter with a center-tapped transformer. V_p and V_s are the DC voltage sources. C_p is the capacitor of primary side. C_{s1} and C_{s2} are voltage divider capacitors for the secondary side bridge. L_p represents the sum of the primary transformer leakage inductance and optional external inductor. L_s is a center-tapped inductor. The transformer turns ratio is $n=N_1/N_2=N_1/N_3$, where $N_2=N_3$. Here, u_1, u_1, u_2, u_s are the high frequency square wave

National Natural Science Foundation of China (51677162) and Natural Science Foundation of Hebei province (E2015203407; QN20131041)

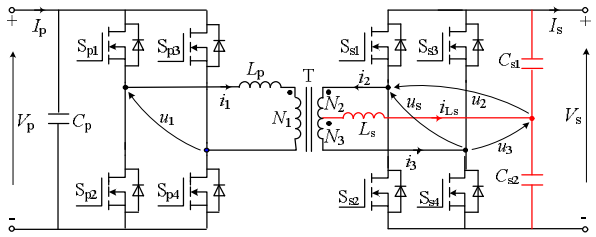

Fig. 1. The improved DAB converter with center-tapped transformer

voltage sources. In order to reach the volt-second balance of the transformer windings within half switching cycle, ϕ_p representing the phase shift between primary side switches is adjusted. The phase shift between secondary side switches is ϕ_s which generates a voltage differential between the center-tapped inductor. The reactive power circulation flowing through L_s provides soft-switching current. The phase shift angle ϕ between primary side and secondary side switches controls the bidirectional power flow.

Fig. 2 shows the derivation process of equivalent circuits for the center-tapped transformer. All the primary-referred parameters are marked with " ′ ". In order to analysis simply, the inductors of Δ equivalent circuit are equal and which is represented by L. And the primary side and center-tapped inductors can be expressed as follows.

$$\begin{cases} L_p = \dfrac{L}{2} \\ L_s = \dfrac{L}{6n^2} \end{cases} \tag{1}$$

In order to reach the volt-second balance of the transformer windings within half switching cycle, the inner phase shift angle ϕ_p of primary bridges can be expressed as follows.

$$\phi_p = \pi\left(1-\frac{1}{2k}\right) \tag{2}$$

Where, k is the voltage gain of converter and can be defined as follows.

$$k = \frac{V_p}{nV_s} \tag{3}$$

According to the voltage rising sequence of u_1, u_2 and u_3, the operating situation is divided into four modes. With TPSFF control, modes I, II, III are for light load condition. And in mode IV, EPSVF control is used for heavy load condition. Fig. 3 shows the idealized operating waveforms of each positive operating mode.

Through the detailed analysis of the steady state operating process, the expressions of current and power can be derived in the four modes, respectively. The normalized power transfer e-

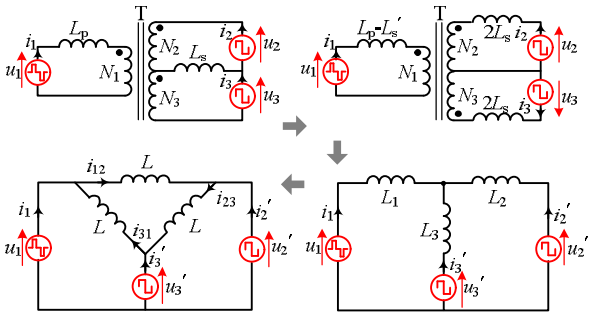

Fig. 2. Derivation process of equivalent circuits

quations are expressed as follows. And the curve of normalized power versus secondary phase shift ϕ_s and phase shift ϕ is drawn in Fig. 4.

$$P^* = \begin{cases} \dfrac{2\phi(\pi-\phi_s)}{\pi-\phi_p} & \text{Mode I} \\ 2\phi & \text{Mode II} \\ \dfrac{4\phi(2\pi-\phi-\phi_s-\phi_p)-(\phi_p-\phi_s)^2}{4(\pi-\phi_p)} & \text{Mode III} \\ \dfrac{4\phi(\pi-\phi)-\phi_p^{\,2}}{2(\pi-\phi_p)} & \text{Mode IV} \end{cases} \tag{4}$$

Where, the base values of normalized current and power are expressed as follows.

$$\begin{cases} I_{base} = \dfrac{nV_s}{2\omega L} \\ P_{base} = \dfrac{n^2V_s^{\,2}}{4\omega L} \end{cases} \tag{5}$$

Table I shows the normalized switching currents of each mode. When the phase shift angle of the secondary side switches is zero, the mode I, II, III can be normalized to mode II and the worst soft-switching current equals to zero. Furthermore, considering the effect of the parasitic parameters and dead time, the charging and discharging process of the parasitic capacitors cannot be completed within the dead time. In practice the soft switching cannot be achieved at the secondary side. As can be seen in the table I, the minimum soft-switching currents in mode I, II and III are equal and the normalized soft-switching current is $-\phi_s$ by adopting TPSFF control mentioned previously. Thus, only adjusting the value of phase shift between the secondary switches can change and set the worst soft-switching current value. In case the minimum soft-switching current is set to -2A, the phase angle ϕ_s is 0.126π. It brings little effect on the output power because the ϕ_s is small.

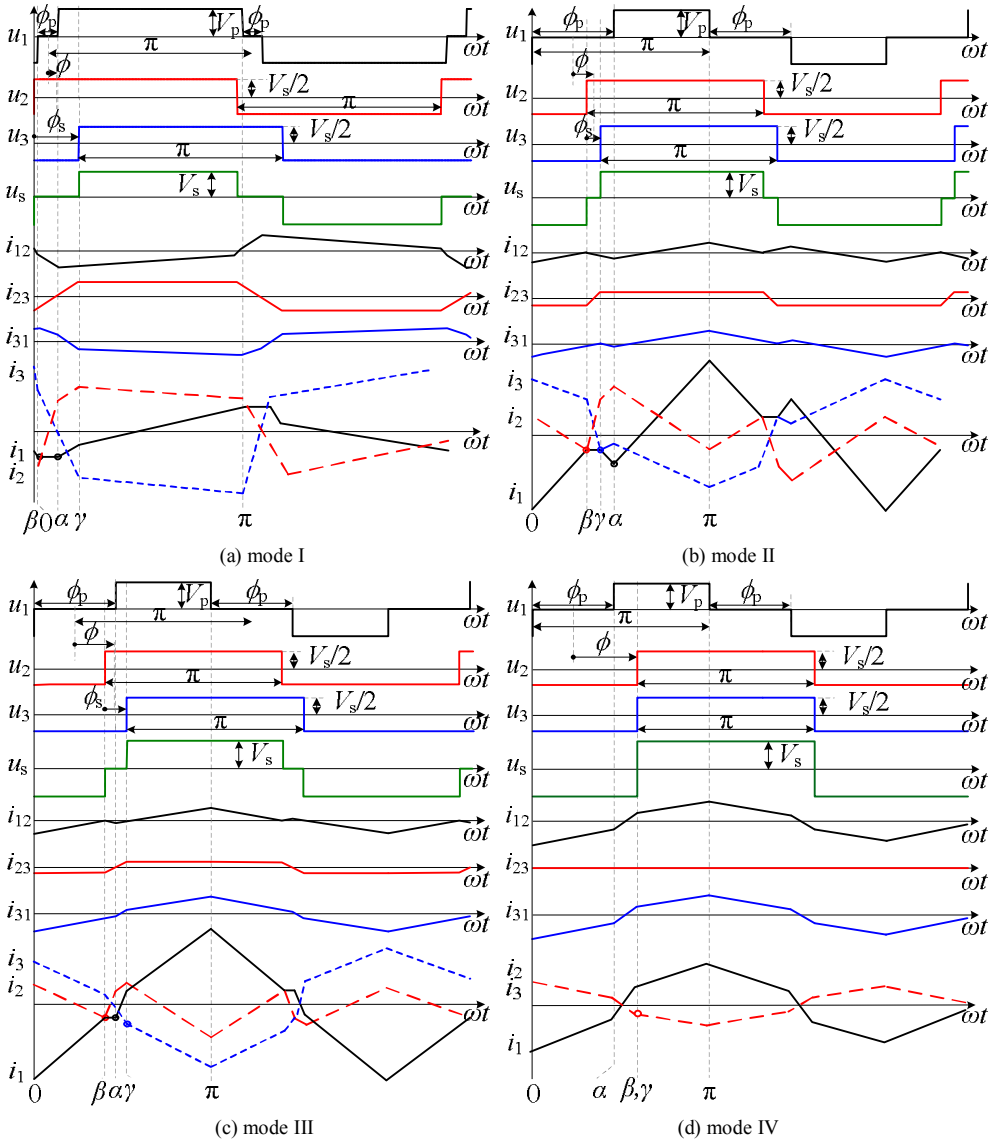

Fig. 3. Idealized operating waveforms

TABLE I. SWITCHING CURRENTS IN ALL OPERATING MODES

	Mode I	**Mode II**	**Mode III**	**Mode IV**
	$0\le\phi\le(\phi_s-\phi_p)/2,\ \phi_p\le\phi_s$	$0\le\phi\le(\phi_p-\phi_s)/2,\ \phi_s\le\phi_p$	$\lvert\phi_p-\phi_s\rvert/2\le\phi\le(\phi_p+\phi_s)/2$	$(\phi_p+\phi_s)/2\le\phi\le\pi/2,\ \phi_s=0$
$i_1^*(0)$	$-\phi_s$	$-\phi_p-2\phi\le-\phi_s$	$-\phi_p-2\phi\le-\phi_s$	$-\phi_p-2\phi\le i_2'^*(\beta)$
$i_1^*(\alpha)$	$-\phi_s$	$-\phi_p+2\phi\le-\phi_s$	$-\phi_s$	$\phi_p-2\phi\le i_2'^*(\beta)$
$i_2'^*(\beta)$	$\pi(\phi_p+2\phi-\phi_s)/(2\pi-2\phi_p)$ $-\phi_s\le-\phi_s$	$-\phi_s$	$-\phi_s$	$\pi(\phi_p-2\phi)/(2\pi-2\phi_p)$
$i_3'^*(\gamma)$	$\pi(\phi_p-2\phi-\phi_s)/(2\pi-2\phi_p)$ $-\phi_s\le-\phi_s$	$-\phi_s$	$\pi(\phi_p-2\phi-\phi_s)/(2\pi-2\phi_p)$ $-\phi_s\le-\phi_s$	$\pi(\phi_p-2\phi)/(2\pi-2\phi_p)$
i_{wst}^*	$i_1^*(0),\ i_1^*(\alpha)=-\phi_s$	$i_2'^*(\beta),\ i_3'^*(\gamma)=-\phi_s$	$i_1^*(\alpha),\ i_2'^*(\beta)=-\phi_s$	$i_2'^*(\beta),\ i_3'^*(\gamma)$
Bridges with i_{wst}^*	S_{p1}-S_{p2}, S_{p3}-S_{p4}	S_{s1}-S_{s2}, S_{s3}-S_{s4}	S_{p3}-S_{p4}, S_{s1}-S_{s2}	S_{s1}-S_{s2}, S_{s3}-S_{s4}

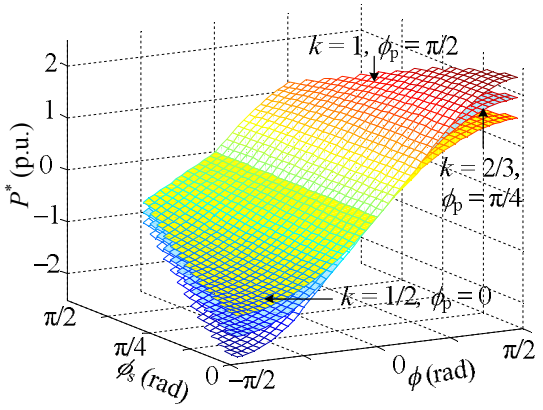

Fig. 4. P^* versus ϕ_s and ϕ according to different k and ϕ_p

III. Phase Shift and Variable Frequency Control

At the light load, the soft-switching current reaches the set value with TPSFF control. With the increasing of the output power, the converter enters model IV and the worst soft-switching current increases. Then, the optimized target is changed from complete soft switching to restrict the reactive current. In model IV, there is no current flow through the center-tapped inductor because ϕ_s is set to zero. Adding variable-frequency control can make the worst soft-switching current to the set value and achieve the complete ZVS with the minimum reactive current compared with the fixed frequency control.

In mode IV, the worst soft-switching current is $i_2^{'*}(\beta)$. Here, we define I_{zvs} is the value of the worst soft-switching current. and I_{out} is the average value of the output current. So, the equation is obtained as follows.

$$\begin{cases} I_{zvs} = i_2^{'*}(\beta) * I_{base} \\ I_{out} = P^*(\text{IV}) * P_{base} / V_s \end{cases} \tag{6}$$

Combining with (4), (5) and (6), the expressions of the switching frequency f_s and the phase shift angle ϕ can be derived as follows.

$$\begin{cases} f_s = \dfrac{-[\pi I_{out} + I_{zvs}(\pi - \phi_p)] + A}{8nLI_{zvs}{}^2(\pi - \phi_p)/V_s} \\ \phi = \dfrac{\pi(I_{out} + I_{zvs}) - A}{2I_{zvs}} \\ \text{where, } A = \sqrt{\pi^2 I_{out}{}^2 + 2\pi I_{zvs} I_{out}(\pi - \phi_p) + I_{zvs}{}^2(\pi^2 - \phi_p{}^2)} \end{cases} \tag{7}$$

The curves of switching frequency f_s and phase shift angle ϕ versus output current I_{out} according to different ϕ_p are drawn in Fig. 5. The soft-switching current values of the solid curves and the dotted curves are set to -2A and -3A, respectively. In order to protect hardware of the converter, the switching frequency is limited to 50-200 kHz. When the switching frequency is beyond the range, it can be return to normal range by raising or decreasing the value of I_{zvs}.

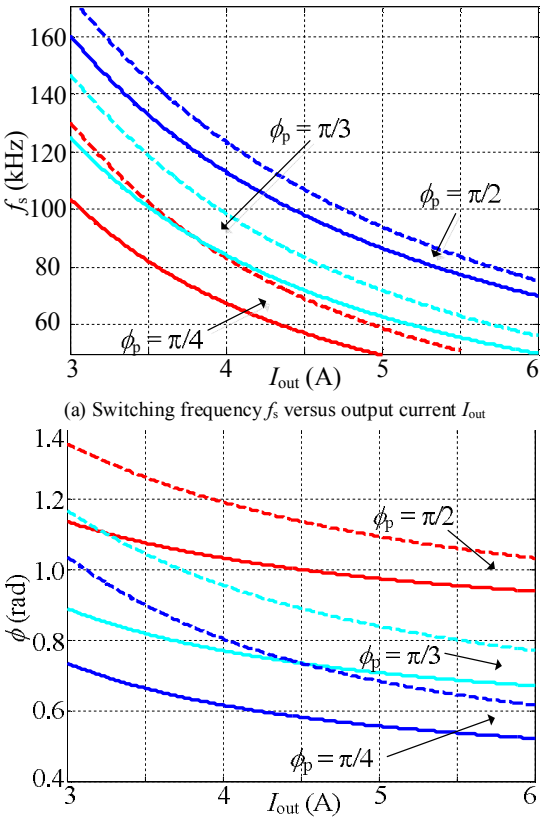

(a) Switching frequency f_s versus output current I_{out}

(b) Phase shift angle ϕ versus output current I_{out}

Fig. 5. f_s and ϕ versus I_{out} according to different ϕ_p

IV. Experimental Verification

A 1.1kW prototype is established to verify the correctness of the theoretical analyses. Table II shows the parameters of the converter. When the dead time is constant, the larger the parasitic capacitance of the switch is, the larger the value of reverse current required to realize ZVS is. The concrete relationship between parasitic capacitance and minimum soft-switching current is not within the range of the study in this paper. As an illustrate, the worst soft-switching current is set to -2A in the experiment to verify the ZVS achievement of all the switches at the whole load range. The experimental results are shown as follows.

TABLE II. Parameters of The Converter

Parameters	Values	Parameters	Values
V_p	120-240V	V_s	240V
L_p	21μH	L_s	7μH
N_1:N_2	21:21	N_1:N_3	21:21
f_s	50kHz~200kHz	P_o	1.1kW

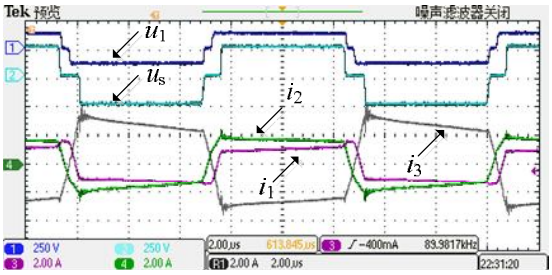

(a) Mode I: V_p=137V, P_o=100W.

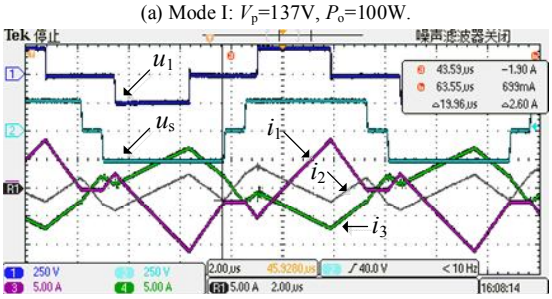

(b) Mode II: V_p=240V, P_o=300W.

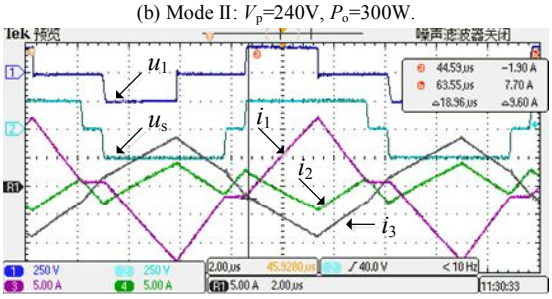

(c) Mode III: V_p=240V, P_o=420W.

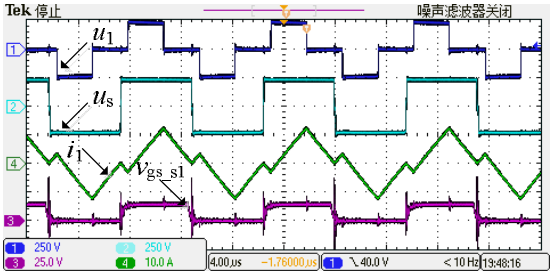

(d) Mode II: ϕ_s=0, V_p=240V, P_o=570W.

Fig. 6. Measured operating waveforms in mode I, II, III

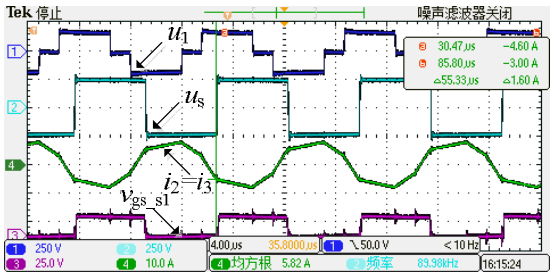

(a) Mode IV: f_s=90kHz, P_o=1.1kW.

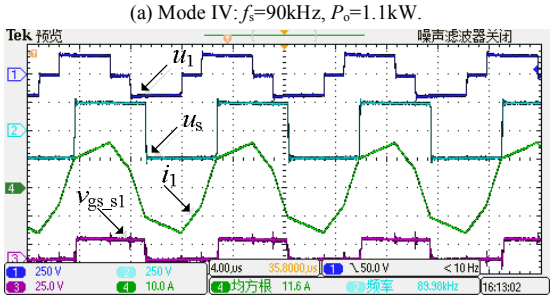

(b) Mode IV: f_s=90kHz, P_o=1.1kW.

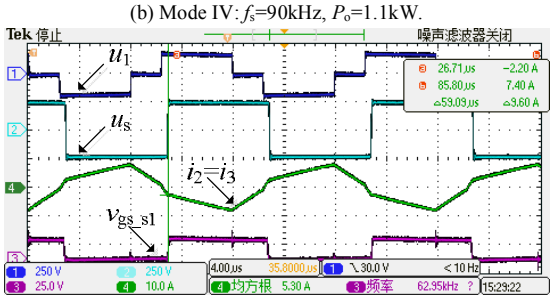

(c) Mode IV: f_s=63kHz, P_o=1.1kW.

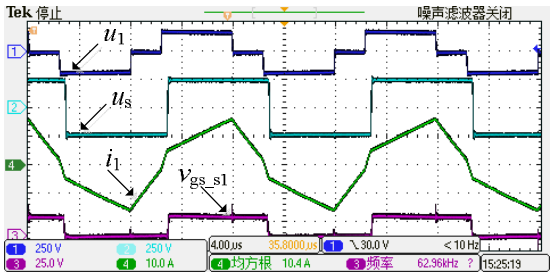

(d) Mode IV: f_s=63kHz, P_o=1.1kW.

Fig. 7. Measured operating waveforms in mode IV

In the Fig.6 (a), (b) and (c), the experimental waveforms of mode I, II, III with FFTPS control are given, where, V_s=240V, f_s=90kHz. By adjusting the phase shift angle of secondary side switches, the worst soft-switching currents measured in the experiment are all -1.9A which is close to the set value. It can be ensured that all the switches can achieve ZVS. Fig.6 (d) shows the operating waveforms where ϕ_s is zero as a special case of mode II. As can be seen, the worst soft-switching current is zero, and in practice the switches of secondary side can't realize the soft switching. The correctness of the above theoretical analysis is verified.

Fig.7 shows the experimental waveforms of mode IV with VFEPS control, where ϕ_s=0, V_p=180V, V_s=240V. In the Figs. 7 (a) and (b), the switch frequency which is unchanged equals to 90 kHz. It can be seen that the worst soft-switching current value is 4.6 A, and the root mean square values of primary and secondary current are 11.6 A and 5.825 A, respectively. As the experimental results shown in the Fig. 7 (c) and (d), the worst soft-switching current value is 2.2 A by adjusting the switch frequency to 63 kHz under the same output power. And the root mean square values of primary and secondary current are reduced to 10.4 A and 5.3 A, respectively. Adopting EPSVF control in mode IV brings that all of the switches realize ZVS and the primary and secondary currents are optimized. Furthermore, the efficiency of the converter is increased from 91.3% to 93.7%.

Fig.8 shows the efficiency curves of the converter under different input voltages with the modified phase shift and variable frequency control, and the maximum efficiency is 95%.

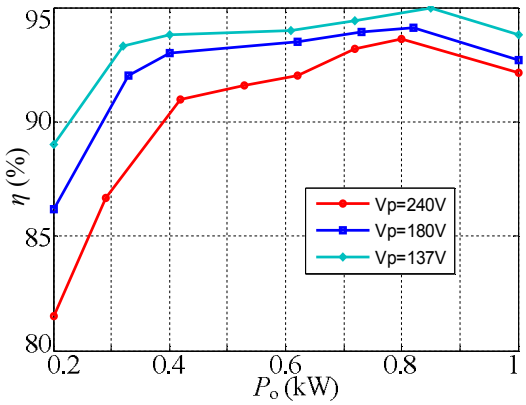

Fig. 8. Efficiency of the converter under different input voltages

V. CONCLUSION

A modified phase shift and variable frequency control scheme is proposed in this paper. The TPSFF control is adopted at light load. The center-tapped inductor at the secondary side can provide the extra soft-switching current for the switches. The worst soft-switching current is the set value to ensure all switches can achieve soft switching, and at the same time, the reactive power is restricted. In order to control the worst soft-switching current as the set value and decrease the reactive power, the EPSVF control is employed at heavy load.

The improved DAB converter employed the proposed control scheme is appropriate to use in the occasion where has wide input voltage range, such as the renewable energy system. The proposed control scheme works out the less soft-switching current at light load and the too large reactive power at heavy load, which increase the reliability and practicability of the converter.

REFERENCES

[1] De Doncker R W A A, Divan D M, Kheraluwala M H. A three-phase soft-switched high power density dc/dc converter for high power applications[C]//Industry Applications Society Meeting, 1988:796-805.

[2] Lu Yangjun, Xing Yan, Wu Hongfei. Dual-phase-shift controlled high step-up soft switching isolated Buck/Boost converter for wide voltage range applications[J]. Transactions of China Electrotechnical Society, 2016, 31(13):10-17.

[3] Kheraluwala M H, Gascoigne R W, Divan D M, et al. Performance characterization of a high-power dual active bridge DC-to-DC converter[J]. IEEE Transactions on Industry Applications, 1992, 28(6):1294-1301.

[4] Liu D, Li H. A ZVS bi-directional DC/DC converter for multiple energy storage elements[J]. IEEE Transactions on Power Electronics, 2006, 21(5):1513 - 1517.

[5] Hosseini S H, Sabahi M, Goharrizi A Y. Multi-function zero-voltage and zero-current switching phase shift modulation converter using a cycloconverter with bi-directional switches[J]. IET Power Electronics, 2008, 1(2):275-286.

[6] Peng F Z, Li H, Su G J, et al. A new ZVS bidirectional DC-DC converter for fuel cell and battery application[J]. IEEE Transactions on Power Electronics, 2004, 19(1):54-65.

[7] Inoue S, Akagi H. A bi-directional isolated DC/DC converter as a core circuit of the next-generation medium-voltage power conversion system[J]. IEEE Transactions on Power Electronics, 2006, 22(2):1-7.

[8] Zhao Biao, Yu Qingguang, Sun Weixin. Bi-directional full-bridge DC/DC converters with dual-phase-shifting control and its backflow power characteristic analysis[J]. Proceedings of the CSEE, 2012, 32(12):43-50.

[9] Jain A K, Ayyanar R. PWM control of dual active bridge: comprehensive analysis and experimental verification[J]. IEEE Transactions on Power Electronics, 2011, 26(4):1215-1227.

[10] Cheng Hong, Gao Qiaomei, Zhu Jinbiao, et al. Dynamic modeling and minimum backflow power controlling of the bi-directional full-bridge DC-DC converters based on dual-phase-shifting control[J]. Transactions of China Electrotechnical Society, 2014, 29(3):245-253.

[11] Wang Cong, Sha Guanglin, Wang Jun. The analysis of zero voltage switching dual active bridge DC/DC converters based on dual phase shift control[J]. Transactions of China Electrotechnical Society, 2015, 30(12):106-113.

[12] Kasper M, Burkart R M, Deboy G, et al. ZVS of power MOSFETs revisited[J]. IEEE Transactions on Power Electronics, 2016, 31(12): 8063-8067.

[13] Hiltunen J, Vaisanen V, Juntunen R, et al. Variable-frequency phase shift modulation of a dual active bridge converter[J]. IEEE Transactions on Power Electronics, 2015, 30(12):7138-7148.

[14] Bai H, Mi C. Eliminate Reactive Power and Increase System Efficiency of Isolated Bidirectional Dual-Active-Bridge DC–DC Converters Using Novel Dual-Phase-Shift Control[J]. IEEE Transactions on Power Electronics, 2008, 23(6):2905-2914.

[15] Oggier G G, Garcia G O, Oliva A R. Switching control strategy to minimize dual active bridge converter losses[J]. IEEE Transactions on Power Electronics, 2009, 24(7):1826-1838.

[16] Wang Yubin, Wang Shanshan, Fengbo. Optimal current control strategy of Dual-active-bridge DC/DC converter based on dual-phase-shift control[J]. Transactions of China Electro technical Society, 2015, 30(14): 488-496.

[17] Shen Y, Sun X, Li W, et al. A modified dual active bridge converter with hybrid phase-shift control for wide input voltage range[J]. IEEE Transactions on Power Electronics, 2016, 31(10):6884-6900.